High-energy direct photoelectron spectroscopy in strong-field ionization

Pei-Lun He,[1,2] Michael Klaiber,[1] Karen Z. Hatsagortsyan,[1,*] and Christoph H. Keitel[1]
[1]*Max-Planck-Institut für Kernphysik, Saupfercheckweg 1, 69117 Heidelberg, Germany*
[2]*Key Laboratory for Laser Plasmas of Ministry of Education and Department of Physics and Astronomy, Collaborative Innovation Center of IFSA, Shanghai Jiao Tong University, Shanghai 200240, China*

(Received 13 July 2018; revised manuscript received 23 September 2018; published 26 November 2018)

Recently, in the tunneling regime of strong-field ionization an unexpected Coulomb field effect has been identified by numerical solution of the time-dependent Schrödinger equation [Phys. Rev. Lett. **117**, 243003 (2016)] in photoelectron spectra in the upper energy range of the direct electrons. We investigate the mechanism of the Coulomb effect employing a classical theory with Monte Carlo simulations of trajectories, and a quantum theory based on the generalized eikonal approximation for the continuum electron. The effect is shown to have a classical nature and is due to momentum space bunching of photoelectrons released not far from the peak of the laser field. Moreover, our analysis reveals specific features of the angular distribution of high-energy direct electrons, which can be employed for molecular imaging. For the H_2^+ molecule as an example we show the signatures of the molecule orientation and the molecular structure in the investigated angular distribution.

DOI: 10.1103/PhysRevA.98.053428

I. INTRODUCTION

The Coulomb field of the atomic core plays a significant role for strong-field ionization. For a long time it has been known that it lowers the tunneling barrier and increases the tunneling probability [1–4]. Significant Coulomb effects arise at recollisions [5]. While hard recollisions induce well-known processes of above-threshold ionization [6], high-order harmonic generation [7], and nonsequential double ionization [8], the soft recollisions bring about Coulomb focusing [9–11] and defocusing [12] effects. The Coulomb focusing is responsible for the lately discovered, so-called, low-energy structures (LESs) [13–29].

Recently, another surprising Coulomb field effect has been identified by *ab initio* numerical solution of time-dependent Schrödinger equation (TDSE) [30]. When comparing the numerical solution for the photoelectron spectra with calculations of the first-order Coulomb-free strong-field approximation (SFA) [31–33], several orders enhancement of photoelectron spectra at $2U_p$, i.e., twice the electron ponderomotive energy, has been observed, see also Ref. [34] and a recent experiment in Ref. [35]. In Ref. [30] the effect was analyzed invoking the Coulomb-corrected action along quantum orbits in the complex-time plane. Due to the Coulomb field, the quantum orbit maintains a large imaginary part up to the recollision, which hinted a conclusion that the enhancement is a specific quantum effect, and that separation into sub-barrier motion up to the tunnel exit and subsequent classical motion is an invalid concept. Although the high-energy enhancement in Ref. [30] is connected to the Coulomb field effect, an intuitive understanding remained missing.

The aim of this paper is to clarify the mechanism of the Coulomb effect (CE) in the photoelectron spectrum for high-energy direct electrons. We carry out classical as well as quantum mechanical analysis. The classical analysis employs the classical trajectory Monte Carlo (CTMC) simulations with nonadiabatic initial conditions for the electrons. For the quantum mechanical analysis we put forward a version of Coulomb-corrected strong-field approximation (CCSFA). In the existing CCSFA, such as the trajectory-based CCSFA [36,37], or analytical R-matrix theory [38–40], the Coulomb field of the atomic core is accounted for using the eikonal wave function for the continuum electron. In the latter Wentzel-Kramers-Brillouin (WKB) approximation is applied, with a perturbative treatment of the Coulomb potential in the phase of the wave function. Unfortunately, the eikonal CCSFA has a singularity for the forward rescattering amplitude, which renders the treatment of the discussed Coulomb effect ambiguous cf. [30]. We go beyond the WKB description of the continuum electron, incorporating into the SFA formalism the electron wave function in the, so-called, generalized eikonal approximation (GEA) [41–45]. In GEA the second-order derivatives of the Schrödinger equation are not neglected, in contrast to WKB approximation, which takes into account quantum recoil effects at recollisions with a small impact parameter and removes the Coulomb singularity of the eikonal CCSFA at recollisions. The accuracy of our analytical results are examined in comparison with numerical solutions of TDSE.

First, we show that already CTMC simulations with nonadiabatic initial conditions reproduce qualitatively the CE. We analyze the trajectories yielding high energies and trace the source of the enhancement. It is due to electrons released not far from the peak of the laser field, though with bunching at high energies because of a large, nonuniform Coulomb momentum transfer, which depends on the ionization phase, i.e., the laser phase at the ionization. In contrast to LES, here we deal mostly with Coulomb defocusing, and the enhancement is not due to Coulomb focusing. Although CE is mainly

*Corresponding author: k.hatsagortsyan@mpi-hd.mpg.de

determined by the parameter $\zeta \equiv Z\omega/E_0 > 1$, pointed out already in Ref. [30], with the frequency ω and the amplitude E_0 of the laser field, and the ion charge Z, we find a significant dependence on the ionization potential I_p. The CE is enhanced and has a peak at an intermediate I_p, which is found to be related to restructuring of the topological structure of the initial phase space of the ionized electrons when approaching the regime of over-the-barrier ionization (OTBI). Second, the applied quantum approach with GEA allows us to remove the Coulomb singularity of the eikonal CCSFA at recollisions, and to obtain a reliable quantum description for the photoelectron spectra near the upper energy limit of the direct electrons. The quantum description induces merely a uniform enhancement of the photoelectron spectra compared to the classical result, indicating that the considered CE has a classical nature. Third, we investigate the angular distribution of high-energy direct electrons and show that it has specific features with apparent side lobes. For the H_2^+ molecule, the side lobes are shown to carry signatures of the molecular orientation and the interatomic separation.

II. QUALITATIVE DISCUSSION

Before going to rigorous calculations, we illustrate the mechanism of the CE with the following qualitative discussion. We begin with the first-order SFA amplitude describing the tunnel ionized direct electrons, neglecting the Coulomb effect of the atomic core:

$$M_{\mathbf{p}} \sim \sum_s \exp\left(-i\int_{t_s} dt(\mathbf{p}+\mathbf{A}(t))^2/2 + iI_p t_s\right), \quad (1)$$

where $\mathbf{p}$ is the final momentum, $\mathbf{A}(t) = \mathbf{e}_x(E_0/\omega)\sin(\omega t)$ the vector potential of the linearly polarized laser field, and t_s the time-saddle point of the relevant trajectory. Then, we derive the Coulomb corrected photoelectron momentum distribution by means of nonuniform (depending on the ionization phase) momentum shifting of the first-order momentum distribution:

$$M^C_{\mathbf{p}} = M_{\mathbf{p}-\mathbf{p}_C}, \quad (2)$$

where $\mathbf{p}_C = -Z\int_{t_e}^{\infty} dt\, \mathbf{r}_L(t)/r_L^3(t)$ is the Coulomb momentum transfer to the electron along the laser-driven trajectory $\mathbf{r}_L(t), r_L(t) = |\mathbf{r}_L(t)|$, and $t_e = \mathrm{Re}\{t_s\}$ the ionization time. For the short trajectory p_{xC} is opposite to the final longitudinal momentum p_x, while for the long trajectory they have the same sign. Accordingly, the Coulomb momentum shift increases the probability $|M^C_{\mathbf{p}}|^2$ for the long trajectory, because the electron with a certain final momentum is ionized closer to the laser peak than in the Coulomb free case, and vice verse for the short trajectories. The photoelectron energy distribution via $|M^C_{\mathbf{p}}|^2$ for recolliding long trajectories is shown in Fig. 1(a). The photoelectron spectrum demonstrates a plateaulike behavior up to $2U_p$ energy, similar to the result of Ref. [30], and indicates that CE arises due to the nonuniform Coulomb momentum transfer to the continuum electron along real trajectories. In this case the electrons with final energy around $2U_p$ are tunneled from the atom not near the zero crossing of the laser field, as in the Coulomb free case, but at the laser phases close to the peak of the field with enhanced probabilities.

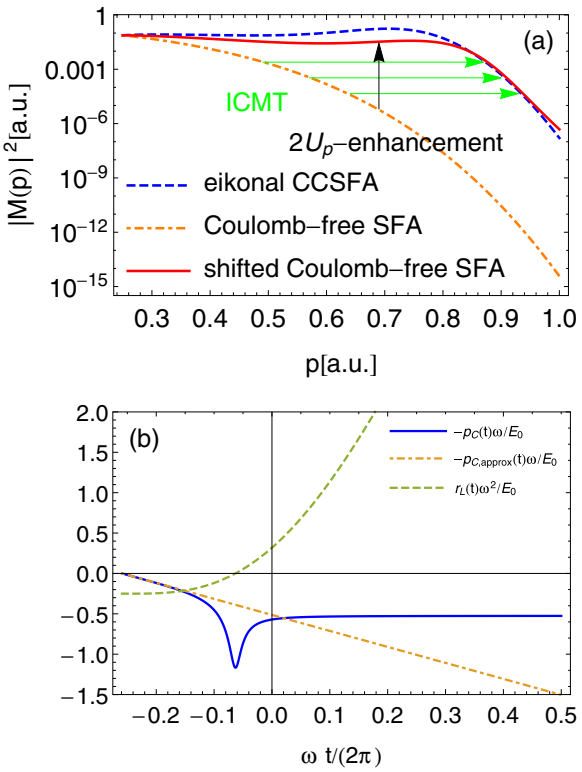

FIG. 1. (a) Photoelectron momentum distribution at a fixed emission angle $\theta = \pi/100$: (red solid) via $|M^C_{\mathbf{p}}|^2$ corresponding to the long trajectory; (blue dashed) via eikonal CCSFA as in Ref. [30]; (orange dot-dashed) the Coulomb-free first-order SFA. The shifts of the momentum distribution due to the initial Coulomb momentum transfer (ICMT) are shown by green arrows, and CE is indicated by a black arrow. (b) Coulomb momentum transfer along the laser field $p_{Cx}(t)/(E_0/\omega)$ vs the interaction time, at $p = 0.69$ and $\theta = \pi/100$: (blue solid) numerical evaluation, (orange dot-dashed) estimation, see the text; (green dashed) the electron trajectory $x(t)/(E_0/\omega^2)$. The parameters are $E_0 = 0.0045$ a.u., $\omega = 0.0065$ a.u., $I_p = 0.14$ a.u., and $Z = 1$.

We can estimate the scaling for CE enhancement analyzing the relevant trajectories. The long trajectory at the $2U_p$ cutoff is launched near zero crossing of the field and the electron is initially almost standing still, further driven by the laser, see a trajectory in Fig. 1(b) (green line), which admits a simple estimate for the Coulomb momentum transfer and the corresponding Coulomb enhancement via

$$\mathcal{E} \equiv \left|M^C_p\right|^2 / |M_p|^2\big|_{E_0/\omega} \sim \exp(4\bar{\zeta}), \quad (3)$$

with the enhancement factor

$$\bar{\zeta} \approx \frac{Z\omega}{E_0}\frac{1}{\gamma^{1/3}}, \quad (4)$$

where $\gamma = \omega\sqrt{2I_p}/E_0$ is the Keldysh parameter, see the derivation in Appendix.

The ratio $\mathcal{R}$ of ionization probabilities at $2U_p$ to U_p can be regarded as a signature of CE to be proved in an experiment (U_p is used as a reference point to avoid the spikes in the spectrum due to LES), which is also determined by the parameters $\bar{\zeta}$, see Appendix.

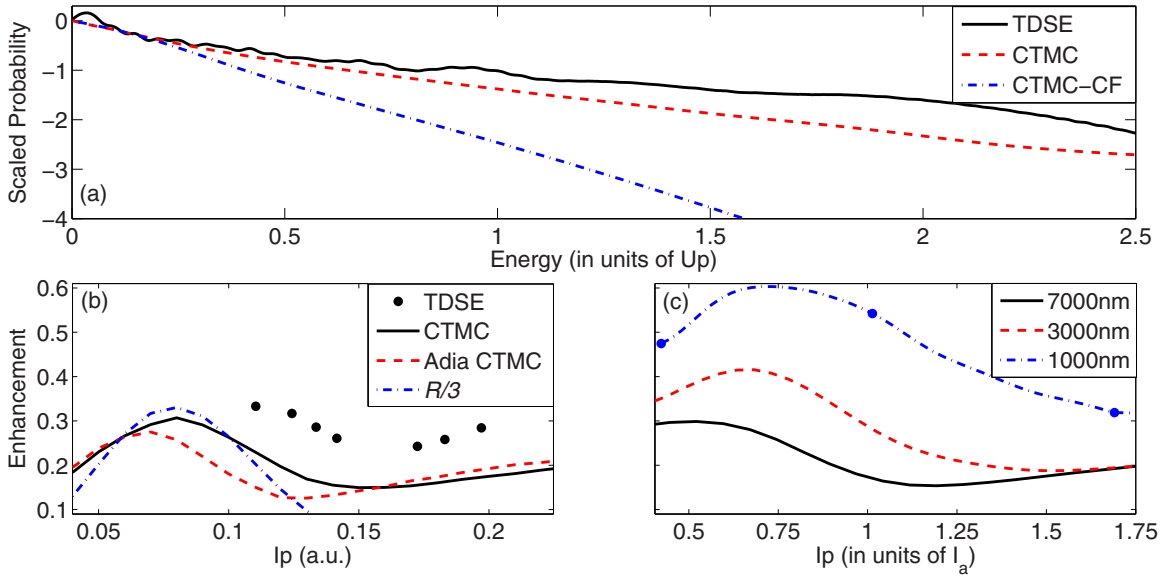

FIG. 2. (a) Photoelectron spectra: (black solid) numerical solution of TDSE, (red dashed) CTMC, (blue dot-dashed) Coulomb-free CTMC. The laser and atom parameters are as in Fig. 1. The ratio $\mathcal{R}$ of ionization probabilities at $2U_p$ to U_p: (b) vs I_p at $E_0 = 0.0045$, $\omega = 0.0065$ a.u. and $Z = 1$, employing a (black solid) CTMC nonadiabatic, (red dashed) CTMC adiabatic, (cycles) TDSE, (dot-dashed) scaled estimation for $\mathcal{R}$, see the text; (c) vs I_p/I_a for different wavelengths at $Z\omega/E_0 = 1.44$, $I_a = \sqrt{4ZE_0}$. The electron initial and final phase space for the points indicated by blue cycles are shown in Fig. 4.

III. CLASSICAL DESCRIPTION

To corroborate the classical nature of CE, we have carried out CTMC simulations with nonadiabatic initial conditions [46]. The latter are favorable for the enhanced Coulomb effect, because the tunnel exit in this case is closer to the core and an initial longitudinal momentum appears, which increases the time the electron spent near the tunnel exit. One can deduce from Fig. 2(a) that the classical simulation shows already the enhancement stemming from the Coulomb field effect and fits qualitatively to the numerical solution of TDSE.

Further, we analyze the dependence of the enhancement on the laser and atom parameters, see Figs. 2(b), 2(c). As a characteristic of the enhancement we use the ratio $\mathcal{R}$ of the probability at energy $2U_p$ to that at the energy U_p. While the parameter $\overline{\zeta}$ qualitatively describes the decreasing behavior of CE with moving I_p far from the peak. However, we find that the enhancement additionally depends on the laser wavelength, and crucially on the ionization potential. The CE is peaked at around $I_p \approx I_a = \sqrt{4ZE_0}$ a.u., when the transition to OTBI takes place [47] and the enhancement character qualitatively changes.

For intuitive understanding of the enhancement mechanism we investigate the initial momentum space $(p_{\perp i}, \phi_i)$ of the trajectories that contribute to CE within the final energy interval of $(1.9U_p, 2.1U_p)$, see Fig. 4. In the Coulomb-free case the contribution to the $2U_p$ energy is not large because either the initial transverse momentum $p_{\perp i}$ is large, or the ionization phase is far from the peak value $\phi_i = 0$, see the red ellipse in the second row of Fig. 4. In contrast to that, when the Coulomb field is accounted for, the electrons contributing to the final $2U_p$ energy range are ionized with smaller $p_{\perp i}$ and ϕ_i (i.e., closer to the peak of the field) with enhanced ionization probabilities.

The typical parameter regime of CE corresponds to Figs. 4(b), 4(e). The dominating CE contribution comes from trajectories B [a typical trajectory is shown in Fig. 1(b)]. Moving along the initial phase structure of B from small values of ϕ_i and $p_{\perp i}$ to the larger ones, corresponds to transition from the wings of the final $2U_p$ energy ring to the central spot at $p_\perp = 0$ in Fig. 4(e). For the former, the final large energy is achieved due to a large transverse Coulomb momentum transfer at a recollision, while for the latter due to an initial Coulomb momentum transfer at the tunnel exit. In this parameter regime the density of the initial phase space for A and C is small.

Thus, when increasing I_p the Coulomb momentum transfer diminishes, $p_C \propto I_p^{-5/3}$ [see Eq. (A12)], and the initial phase space of trajectories B moves far from $\phi_i = 0$, cf. Figs. 4(b) and 4(c), which decreases CE. The maximum of the enhancement is achieved when the left edge of ϕ_i of the initial phase space for B reaches $\phi_i = 0$. At the further decrease of I_p, see Fig. 4(a), the contributing part of the initial phase space crosses the peak, the topological structure of the initial phase space is modified, and the phase space of trajectories A, B, and C are merged. This results in the increase of $p_{\perp i}$, which again suppresses CE. The change of the structure of the initial phase space at decreasing the ionization potential is related to the transition of ionization from the tunneling to the over-the-barrier ionization.

While in LES the enhancement is due to Coulomb focusing, in CE this plays a minor role. We classify the trajectories as Coulomb focused if $|p_{\perp i}| > |p_{\perp f}|$, otherwise Coulomb defocused. In the first case the asymptotic transverse momentum space of the ionized electron is shrunk with respect to that at the tunnel exit, which leads to an additional enhancement and vice versa in the case of defocusing. When classifying

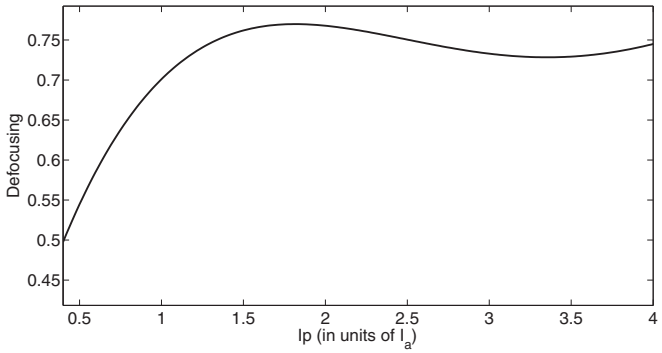

FIG. 3. Weight of defocused trajectories in the case of $E_0 = 0.0045$, $\omega = 0.0065$.

trajectories as focused and defocused we observe that Type B trajectories mostly responsible for CE. These are defocusing trajectories when initial transverse velocity is small. Type C trajectories are Coulomb defocused. Type A trajectories are weakly chaotic and contain both focusing and defocusing electrons. The weight of defocused trajectories in CE is large, see Fig. 3.

IV. MOLECULAR IMAGING

From Figs. 4(g)–4(i) one can see that the angular distribution of photoelectrons at $2U_p$ energies has specific features with wings, especially pronounced at the maximum of the enhancement at $I_p \approx I_a$, when well-defined lobes develop on the wings. The latter feature has a potential to be applied for molecular imaging. We investigate using CTMC simulations, the structure of the angular distribution of CE for a H_2^+ molecule at different orientations of the molecule and at different interatomic separations. The results presented in Fig. 5 show that the relative intensity of the lobes can be a measure of the orientation of the molecule. Moreover, the intensity of the wing tail of the angular distribution (at angles larger than the lobe) carries the signature of the interatom separation in the molecule. This is an example of high-energy direct electron spectroscopy applied to molecular imaging. The latter also hints on a possible experimental demonstration of the considered CE. One may apply a pump-probe scheme, where the first pulse induces the molecule dissociation, while the second one probes the increasing nuclear distance with a variable time delay, using the angular distribution feature of Fig. 5(b).

V. POSSIBILITY OF THE COULOMB ENHANCEMENT OBSERVATION IN A TWO-COLOR LASER FIELD

There are several ways for experimental observation of the discussed CE, when the photoelectron momentum distribution show an enhancement near $2U_p$ energy with respect to the Coulomb free calculations. Two of them are discussed in the paper: first, via the ratio $\mathcal{R}$ of the photoelectron number at $2U_p$ energy to that at U_p, see Figs. 2(b), 2(c) of the paper, and second, via mapping of the molecular orientation into the intensity of the angular distribution lobes, see Fig. 4(a) of the paper. There is a third way for the observation via the use of a two-color orthogonal laser field:

$$E_x = E_1 \cos(\omega t) \tag{5}$$

$$E_y = E_2 \cos(2\omega t + \phi). \tag{6}$$

We employ $E_1/E_2 = 4$ with a variable phase difference ϕ. The angular distribution of the electrons at $2U_p$ energies depends on the phase difference between the fields, see Fig. 6, due to which the energy distribution of photoelectron along

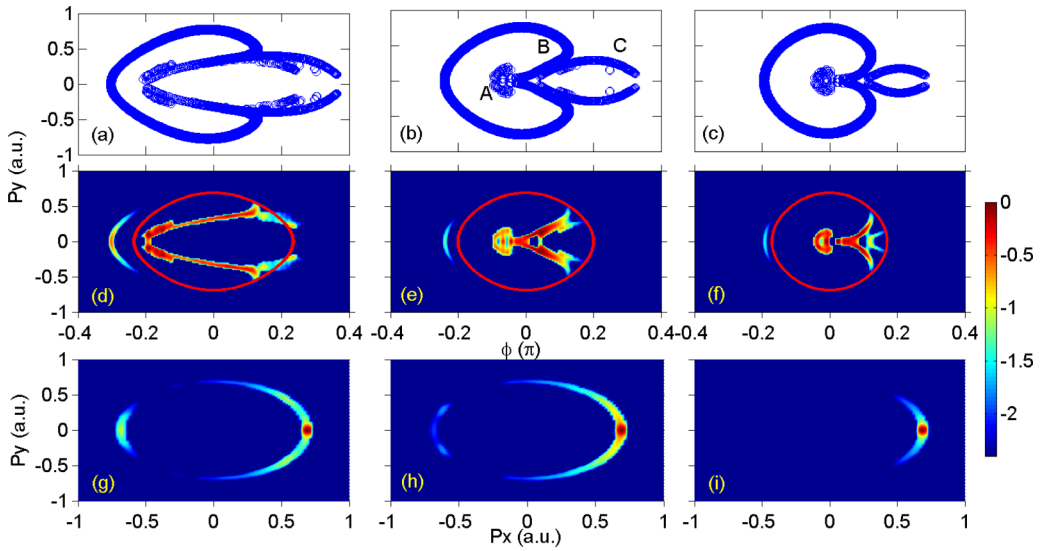

FIG. 4. The electron initial phase space $(p_{\perp i}, \phi_i)$, which finally contributes to the photoelectron energy interval $(1.9U_p, 2.1U_p)$ (first row), with color-coded probabilities (second row): (left column) $I_p = 0.42I_a$ [before the CE peak, indicated in Fig. 2(c) by blue cycle]; (middle column) $I_p = 0.79I_a$ [near the CE peak, indicated in Fig. 2(c) by blue cycle]; (right column) $I_p = 1.35I_a$ [after the CE peak, indicated in Fig. 2(c) by blue cycle]. Asymptotic momentum distribution (third row) for the corresponding I_p values. The phase space of the trajectories A, B, and C type are indicated in the panel (b). The parameters are $E_0 = 0.0315$ a.u., $\omega = 0.0456$ a.u. and $Z = 1$.

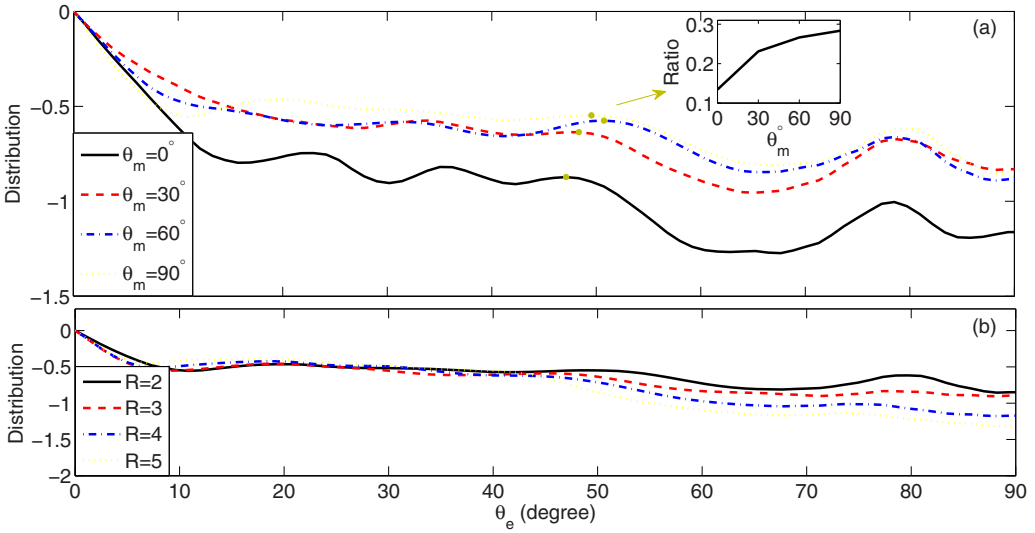

FIG. 5. Photoelectron distribution integrated over the azimuthal angle vs the polar angle θ_e with respect to the laser field direction: (a) in the case of different molecular orientations θ_m of the H_2^+ molecule. The inset shows the ratio of the wing intensity (at the indicated point) to that of the peak. (b) in the case of different inter-atomic separations. The parameters are $E_0 = 0.0315$ a.u. and $\omega = 0.0456$ a.u..

the polarization direction of the strong field E_1 becomes phase dependent, see Fig. 7. The latter can serve as an indicator of the discussed CE. Note that the angle-integrated spectra has no significant phase dependence.

VI. QUANTUM DESCRIPTION. GENERALIZED EIKONAL APPROACH

For the description of CE a nonperturbative treatment of the Coulomb effect is necessary because the perturbative second-order SFA yields uniformly enhanced photoelectron spectra, while at CE the enhancement is large at high energies around $2U_p$. In Ref. [30] CCSFA is applied, which employs eikonal approximation for the electron continuum wave function. The deficiency of this approach is that the ionization amplitude diverges at photoelectron rescattering to small angles, which induces an artificial large contribution to the photoelectron spectra enhancement at high energies, see Fig. 8. We remedy the divergence problem at recollisions using the generalized eikonal wave function in the CCSFA approach, which includes quantum corrections.

The eikonal approximation can be generalized by going beyond the quasiclassical WKB approximation. In GEA the second-order derivatives of the Schrödinger equation are not neglected, in contrast to WKB approximation. The photoelectron momentum distribution in GEA is calculated via the matrix element:

$$M_{\mathbf{p}} = -i \int dt d^3\mathbf{r}\, \psi^{GEA*}(\mathbf{r}, t)\, \mathbf{r} \cdot \mathbf{E}(t)\, \phi(\mathbf{r}, t), \qquad (7)$$

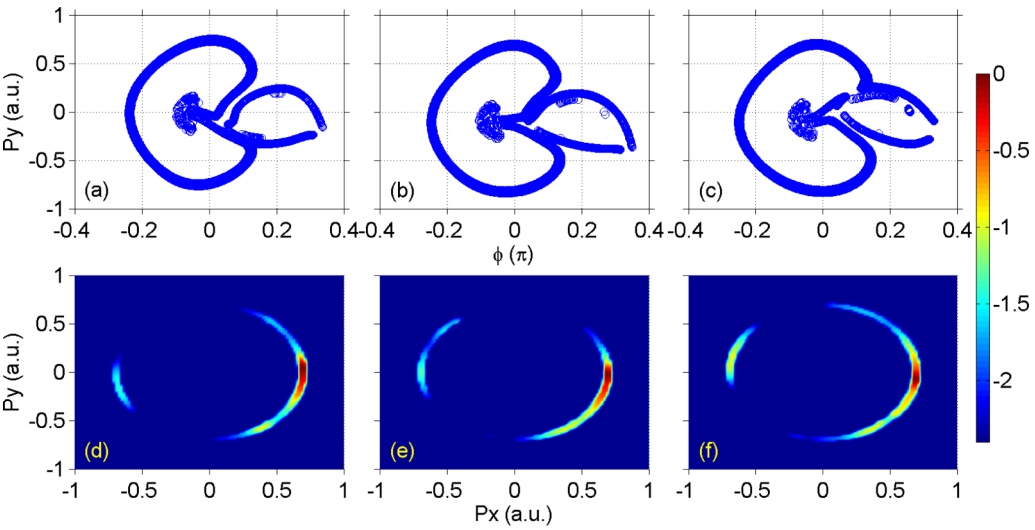

FIG. 6. (a)–(c) The electron initial phase space $(p_{\perp i}, \phi_i)$, which finally contributes to the photoelectron energy interval $(1.9U_p, 2.1U_p)$ in a two-color orthogonal laser field. (d)–(f) Asymptotic momentum distribution. The phase differences between the fields are: (a), (d) $\phi = 0$; (b), (e) $\pi/3$; and (c), (f) $2\pi/3$. The parameters are $E_1 = 0.0315$ a.u., $E_1/E_2 = 4$, $\omega = 0.0456$ a.u., and $I_p = 0.3$ a.u.

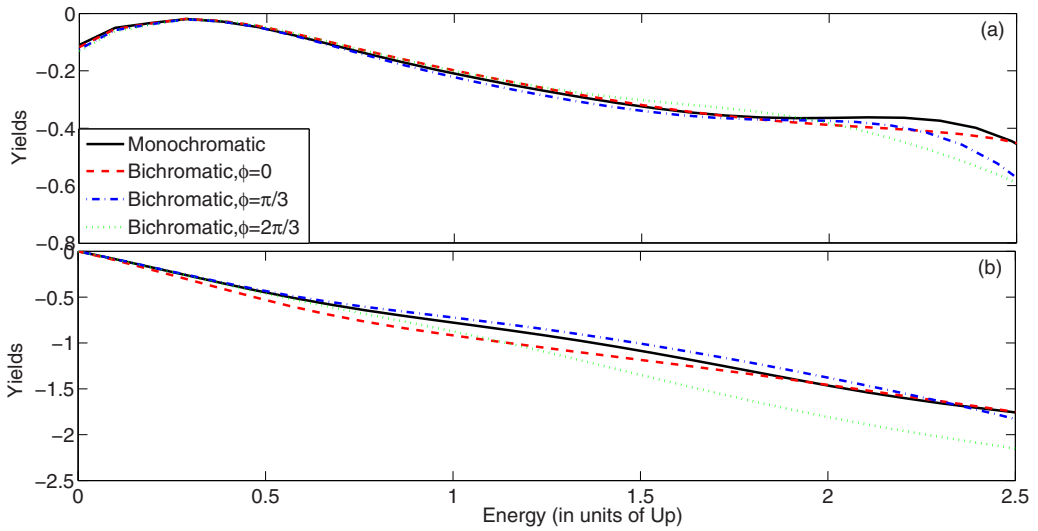

FIG. 7. Photoelectron spectra in a two-color orthogonal field at variable phase difference ϕ between the fields: (a) along the strongest laser polarization; (b) angle-integrated spectra. The parameters are the same as in Fig. 6. $\phi = 0$ (red dashed), $\phi = \pi/3$ (blue dot-dashed), $\phi = 2\pi/3$ (green dotted). For comparison the case of a monochromatic laser field is shown by a solid line.

where $\phi(\mathbf{r}, t)$ is the bound state wave function, and the electron wave function in the continuum $\psi^{GEA}(\mathbf{r}, t)$ accounts the effect of the laser and Coulomb field of the atomic core in GEA [44]:

$$\psi^{GEA}(\mathbf{r}, t) = \exp[iS_0(\mathbf{r}, t) + iS^{GEA}(\mathbf{r}, t)], \tag{8}$$

with the Volkov action

$$S_0 = \int_t dt'(\mathbf{p} + \mathbf{A}(t'))^2/2 + [\mathbf{p} + \mathbf{A}(t)] \cdot \mathbf{r}, \tag{9}$$

and the generalized eikonal

$$S^{GEA}(\mathbf{r}, t) \approx S_1^{GEA}(\mathbf{r}, t) + S_2^{GEA}(\mathbf{r}, t). \tag{10}$$

We calculate the generalized eikonal up to the second order in the scattering potential $V(\mathbf{r})$. The first-order correction to the Volkov action is calculated in Ref. [44]:

$$S_1^{GEA}(\mathbf{r}, t) = \int_t ds V(\mathbf{r}_L(s)) \mathrm{erf}\left[\sqrt{\frac{i\mathbf{r}_L(s)^2}{2(s-t)}}\right]. \tag{11}$$

The second-order terms are defined by the following differential equation

$$-\partial_t S_2^{GEA} = \left(\nabla S_1^{GEA}\right)^2/2 + \nabla S_0^{GEA} \nabla S_2^{GEA} - i\Delta S_2^{GEA}/2 \tag{12}$$

$$\approx \left(\nabla S_1^{GEA}\right)^2/2 + \nabla S_0^{GEA} \nabla S_2^{GEA}. \tag{13}$$

The second equation can be solved by the method of characteristics, which yields the solution

$$S_2^{GEA} \approx \int_t ds \frac{\nabla S_1^{GEA}(s)^2}{2}, \tag{14}$$

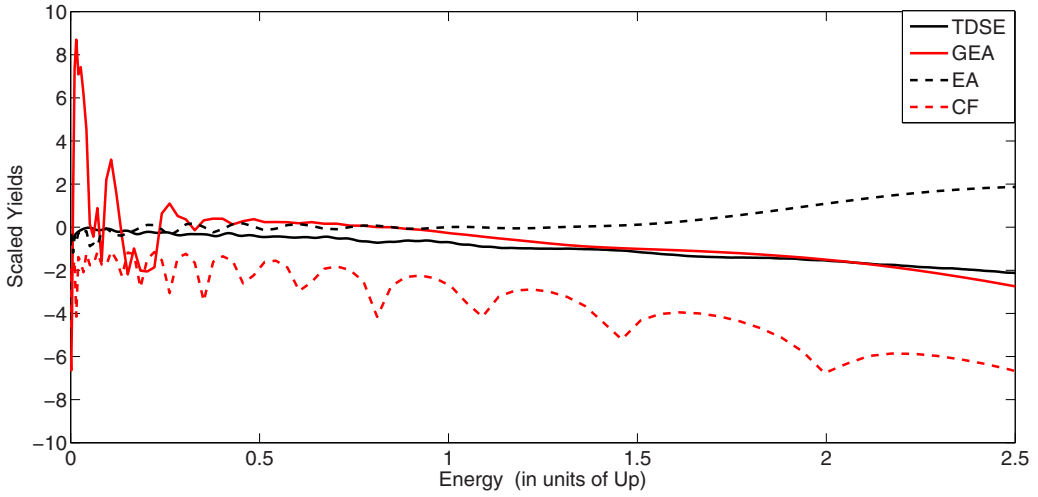

FIG. 8. Photoelectron spectra in logarithmic scale angle integrated within $\pm 6^0$ along the laser polarization direction: (black solid) via numerical TDSE; (red solid) via GEA; (black thick-dashed) via eikonal CCSFA as in Ref. [30]; (red thin-dashed) via Coulomb free SFA. The laser and atom parameters are the same as in Fig. 2.

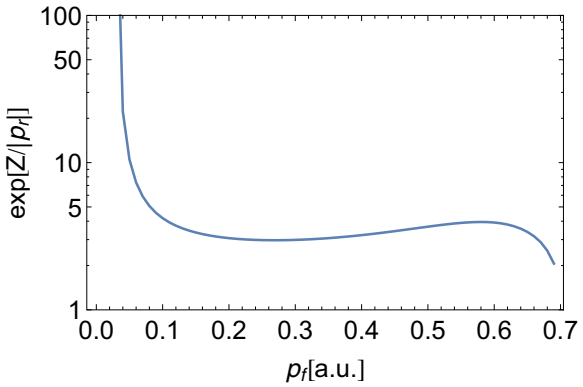

FIG. 9. The estimation of the GEA enhancement vs the final photoelectron momentum p_f; p_r is the recollision momentum.

which finally leads to the second-order GEA correction to the eikonal:

$$S_2^{GEA}(\mathbf{r},t)=\frac{1}{2}\int_t ds\left(\int_s ds'\nabla V(\mathbf{r}_L(s'))\mathrm{erf}\left[\sqrt{\frac{i\mathbf{r}_L(s')^2}{2(s'-t)}}\right]\right)^2. \tag{15}$$

The generalized eikonals of Eqs. (14)–(15) are free from Coulomb singularities and branch points, see also Ref. [48]. We solve the integrals in the amplitude of Eq. (7) with the saddle-point method and expanding the saddle points up to first order in the atomic potential.

The photoelectron spectrum along the laser polarization in GEA is presented in Fig. 8 and shows enhancement with respect to the Coulomb-free case, and the same slope for the spectrum as for the TDSE result. The difference between the quasiclassical eikonal approximation and the GEA occurs at $2U_p$ energies where the quasiclassical approximation is not valid and singular at the forward scattering of the zero angle. The GEA includes quantum corrections, which yields to some enhancement with respect to the eikonal approximation case at energies around U_p. The quantum corrections of GEA are overestimated, which induce not realistic large enhancement of the LES. Below we give qualitative estimation of the GEA enhancement at low energies.

The first-order action term due to the GEA can be estimated at the recollision $t_r \sim 1/\omega$. Assuming that the electron has an impact parameter $y \sim p_{yr}/\omega$ and a longitudinal recollision momentum p_{xr} the error function in the action becomes relevant when $y^2/t_r \ll 1$. Then it can be expanded based on the following relationship for small x: $\mathrm{erf}(x) \sim 2x/\sqrt{\pi}$, yielding

$$S_1^{GEA} \approx -Z\int_t ds\sqrt{\frac{2i}{\pi(s-t)}}. \tag{16}$$

Since the typical time interval when this is true can be estimated by $p_{xr}ds \lesssim \sqrt{s}$ for vanishing y, the action term is of the order of Z/p_{xr}. In Fig. 9 the GEA enhancement parameter $\exp(iS_1^{GEA})$ is plotted against the recollision momentum, displaying the estimate for the GEA enhancement at low energies.

In more intuitive terms, within the ionization time t and the recollision time s, the electron has an energy uncertainty $\Delta\varepsilon \sim 1/(s-t)$, i.e., the momentum uncertainty $\Delta p \sim 1/\sqrt{s-t}$, and the recollision impact parameter is $\rho \sim \Delta p(s-t) \sim \sqrt{s-t}$. The recollision time can be estimated $\Delta s \sim \rho/p_{xr}$, and the GEA phase $\sim Z\Delta s/\sqrt{s-t} \sim Z/p_{xr}$. The latter indicates that GEA overestimates quantum enhancement at slow recollisions when $p_{xr} \approx 0$.

Continuity of the integrand of the eikonal in GEA

The integrand of the eikonal in GEA has the form $I_{GEA} = \mathrm{erf}\sqrt{\mathrm{x}}/\sqrt{\mathrm{x}}$. This function is continuous for all complex x, since the error function can be expanded in the whole complex space via

$$\frac{\mathrm{erf}\sqrt{\mathrm{x}}}{\sqrt{x}}=\frac{2}{\sqrt{\pi}}\sum_{n=0}^{\infty}\frac{(-1)^n x^n}{n!(2n+1)}, \tag{17}$$

which consists only of continuous polynomial functions. Instead the integrand in the eikonal expansion has the simpler form of $I_{EA} = 1/\sqrt{x}$, but has branch cuts, see the three-dimensional plot of the imaginary part of this function in Fig. 10.

One can straightforwardly show how discontinuity in the GEA integrand disappears: $\mathrm{Im}\{\mathrm{I_{GEA}}\} = \mathrm{Re}\{\mathrm{erf}(\sqrt{\mathrm{x}})\}\,\mathrm{Im}\{1/\sqrt{\mathrm{x}}\} + \mathrm{Im}\{\mathrm{erf}(\sqrt{\mathrm{x}})\}\mathrm{Re}\{1/\sqrt{\mathrm{x}}\}$. The imaginary parts of $1/\sqrt{x}$ and $\mathrm{erf}(\sqrt{\mathrm{x}})$ are discontinuous, see Fig. 10, but at the same time they are multiplied by $\mathrm{Re}\{\mathrm{erf}\sqrt{\mathrm{x}}\}$ and $\mathrm{Re}\{1/\sqrt{\mathrm{x}}\}$, respectively, which tends to 0 at the discontinuity of the imaginary parts, see Fig. 10, making the overall function smooth.

Therefore, in contrast to the eikonal approximation, in the GEA it is not necessary to shift the time integration contour in complex plane at recollisions, but can be carried out, for example, along the real time axis.

VII. CONCLUSION

We have demonstrated that the enhancement of the tunnel ionized photoelectron spectra at the upper energy limit of the direct electrons in the strong Coulomb field regime is of a classical origin. We found that the nonuniform Coulomb momentum transfer with respect to the ionization phase allows for the electrons tunneled not far from the peak of the laser field to accumulate at high energies. The enhancement not only depends on the main parameter of the strong Coulomb field regime $Z\omega/E_0$, but also crucially on the ionization potential. We locate a peak of the enhancement with respect to the ionization potential and relate this to the structure of the initial phase space of the contributing electrons. At the peak of the enhancement with respect to the ionization potential the angular distribution shows well distinguishable side lobes, which can be employed to develop a spectroscopy method for molecular imaging. In contrast to LES, the Coulomb focusing plays no role for this enhancement effect.

In an experiment the Coulomb enhancement can be most straightforwardly observed via the ratio of the photoelectron number at $2U_p$ energy to that at U_p. One may use also a

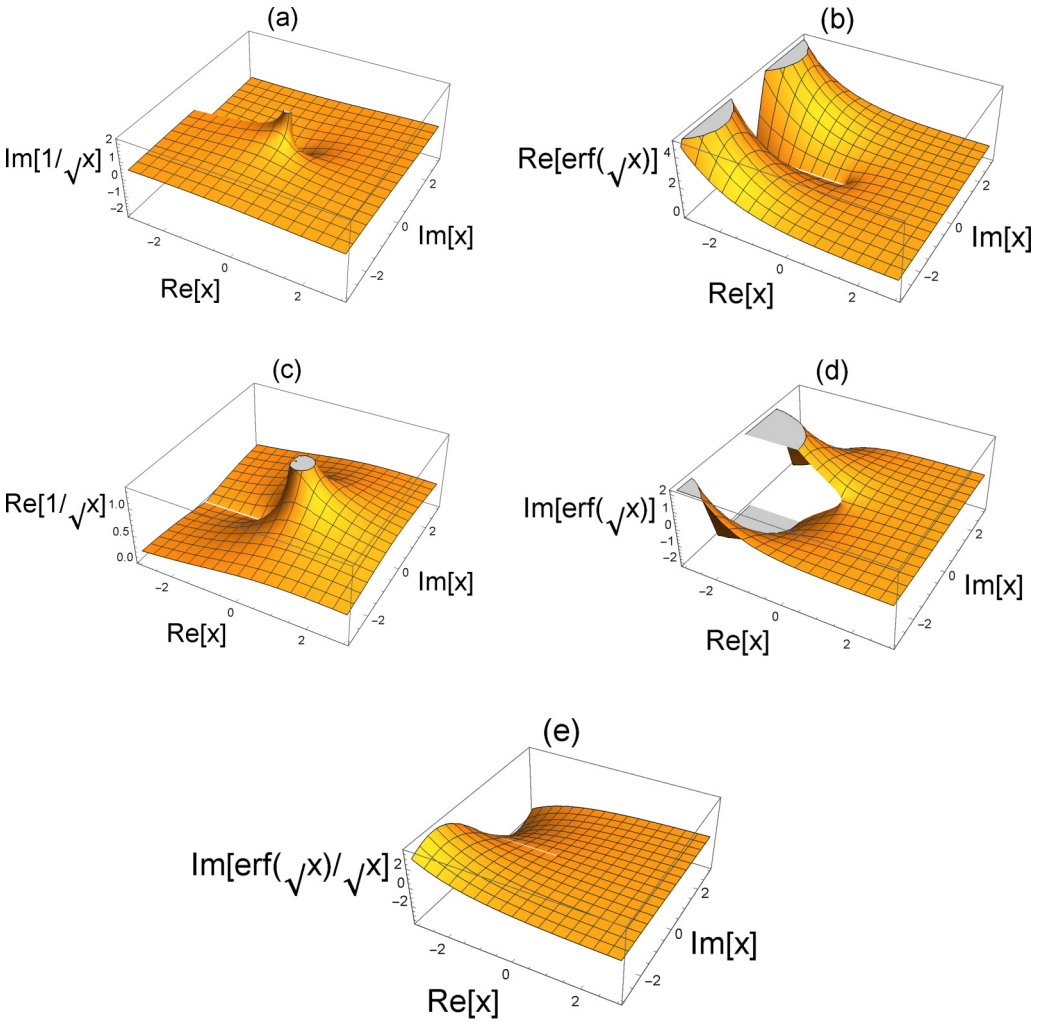

FIG. 10. The continuity of the integrand of the GEA eikonal $I_{GEA} = \mathrm{erf}\sqrt{x}/\sqrt{x}$: (a) The function $\mathrm{Im}\{1/\sqrt{x}\}$ in the complex plane is discontinuous. (b) The function $\mathrm{Re}\{\mathrm{erf}(\sqrt{x})\}$ in the complex plane is continuous. (c) The function $\mathrm{Re}\{1/\sqrt{x}\}$ in the complex plane is continuous. (d) The function $\mathrm{Im}\{\mathrm{erf}(\sqrt{x})\}$ in the complex plane is discontinuous. (e) However, the function $\mathrm{Im}\{\mathrm{erf}(\sqrt{x})/\sqrt{x}\}$ in the complex plane is continuous.

two-color orthogonal laser field, where the Coulomb enhancement is exhibited in the dependence of the photoelectron spectra on the phase difference of the color fields.

For the accurate quantum description of the Coulomb effects at fast recollisions, we put forward a Coulomb-corrected version of SFA based on the generalized eikonal approximation, which is free from Coulomb singularities at recollisions.

ACKNOWLEDGMENT

P.-L.H. acknowledges the support from the China Scholarship Council (CSC).

P.-L.H. and M.K. contributed equally to this work.

APPENDIX: ESTIMATION OF THE COULOMB MOMENTUM TRANSFER AND THE COULOMB ENHANCEMENT FACTOR

We use the laser field

$$E_x(t) = -E_0 \cos \omega t, \tag{A1}$$

with the vector potential:

$$A_x(t) = (E_0/\omega) \sin \omega t. \tag{A2}$$

The electron dynamics can be derived from the canonical momentum conservation:

$$p_x(t) - A_x(t) = -A_x(t_e), \tag{A3}$$

with the ionization time t_e, assuming vanishing longitudinal momentum at the tunnel exit in the Simpleman model [in the applied SFA $t_e = \mathrm{Re}(t_s)$ and there is a nonadiabatic longitudinal momentum at the tunnel exit, which is, however, small at $\gamma < 1$]. The electron momentum is:

$$p_x(t) = \frac{E_0}{\omega}(\sin \omega t - \sin \omega t_e), \tag{A4}$$

and the electron trajectory is:

$$x(t) = -\frac{E_0}{\omega^2}[\omega(t - t_e) \sin \omega t_e + \cos \omega t - \cos \omega t_e] + x_e, \tag{A5}$$

with the tunnel exit $x_e \approx I_p/E_0$. We consider $\omega(t-t_e) \ll 1$ and the electron is assumed to appear in the continuum at the laser phase $\phi_e \equiv \omega t_e$ close to $\pi/2$ ($0 < \phi_e < \pi/2$). Then,

$$\cos\omega t - \cos\omega t_e \approx -\omega(t-t_e)\sin\omega t_e - \cos\omega t_e \frac{\omega^2(t-t_e)^2}{2} + \sin\omega t_e \frac{\omega^3(t-t_e)^3}{6}. \tag{A6}$$

Therefore, the trajectory at $\omega t_e \approx \pi/2 - \epsilon$ ($\epsilon \ll 1$) can be approximated as

$$x(t) \approx -\frac{E_0}{\omega^2}\left[-\sin\epsilon\frac{\omega^2(t-t_e)^2}{2} + \frac{\omega^3(t-t_e)^3}{6}\right] + x_e \approx -\frac{E_0\omega(t-t_e)^3}{6} + x_e, \tag{A7}$$

where we used $\epsilon \sim \omega(t-t_e) \ll 1$. The Coulomb momentum transfer can be estimated

$$p_C \sim F_C \delta t, \tag{A8}$$

with the Coulomb force $F_C \sim Z/x_e^2$, and the effective interaction time δt. The latter is estimated from the condition

$$|x(t_e+\delta t) - x_e| \sim |x_e|, \tag{A9}$$

which reads

$$\frac{E_0\omega\delta t^3}{6} \sim \frac{I_p}{E_0}, \tag{A10}$$

i.e.,

$$\delta t \sim \left(\frac{6I_p}{E_0^2\omega}\right)^{1/3}, \tag{A11}$$

and the Coulomb momentum transfer is derived:

$$p_C \sim Z\left(\frac{6E_0^4}{\omega I_p^5}\right)^{1/3} = 4Z\left(\frac{3}{\gamma}\right)^{1/3}\frac{E_0}{E_a}, \tag{A12}$$

with the atomic field $E_a = (2I_p)^{3/2}$ and the Keldysh parameter $\gamma = \omega\sqrt{2I_p}/E_0$.

The $2U_p$-enhancement factor can be estimated as

$$\mathcal{E} \equiv \left.\frac{|M_p^C|^2}{|M_p|^2}\right|_{p=E_0/\omega}, \tag{A13}$$

with the first-order SFA longitudinal momentum distribution

$$|M_p|^2 \sim \exp(-p^2/\Delta_\parallel^2), \tag{A14}$$

with $\Delta_\parallel = \sqrt{3E_0/E_a}E_0/\omega$, and the Coulomb-corrected ionization amplitude

$$M_p^C = M_{p-p_C}. \tag{A15}$$

The Coulomb enhancement factor is

$$\mathcal{E} = \exp\left(\frac{2p\,p_C}{\Delta_\parallel^2} - \frac{p_C^2}{\Delta_\parallel^2}\right). \tag{A16}$$

The ratio can be estimated

$$\left.\frac{p_C}{p}\right|_{p=E_0/\omega} \approx 4\frac{Z\omega}{E_0}\frac{E_0}{E_a}\left(\frac{3}{\gamma}\right)^{1/3}. \tag{A17}$$

At chosen parameters $E_0 = 0.0045$, $\omega = 0.0065$, and $I_p = 0.14$, one has $p_C/p_0 \approx 0.35$ and $p_0 \equiv E_0/\omega \approx 0.69$. Then, the exponent in Eq. (A16) is mostly determined by the first term:

$$\left.\frac{2p\,p_C}{\Delta_\parallel^2}\right|_{p=E_0/\omega} \approx 4\frac{Z\omega}{E_0}\left(\frac{1}{\gamma}\right)^{1/3}. \tag{A18}$$

Thus, the enhancement factor is

$$\mathcal{E} \sim \exp(4\bar{\zeta}), \tag{A19}$$

$$\bar{\zeta} \approx \frac{Z\omega}{E_0}\frac{1}{\gamma^{1/3}}. \tag{A20}$$

The ratio $\mathcal{R}$ of ionization probabilities at $2U_p$ to U_p can be regarded as a signature of CE to be proved in an experiment (U_p is used as a reference point to avoid the spikes in the spectrum due to LES), which can be estimated in a same way:

$$\mathcal{R} \equiv \frac{|M^C_{E_0/\omega}|^2}{|M^C_{E_0/\sqrt{2}\omega}|^2}. \tag{A21}$$

It is also determined by the parameters $\bar{\zeta}$ (along with E/E_a and γ)

$$\mathcal{R} \approx \exp\left\{\frac{(p_1 - p_{C1})^2 - (p_0 - p_C)^2}{\Delta_\parallel^2}\right) \tag{A22}$$

with $p_0 = E_0/\omega$, $p_1 = E_0/(\sqrt{2}\omega)$, $p_C = 4Z(E_0/E_a)(3/\gamma)^{1/3}$, and $p_{C1} = \pi E_0/E_a$.

Due to Coulomb momentum transfer, the photoelectron with a final energy around the $2U_p$ energy are originated not at $\phi_i = \pi/2$, as in the Coulomb-free case, but at phases closer to the peak of the field: $\phi_i = \pi/2 - \delta\phi_i$. We can estimate the phase of the laser field, which mostly contributes as follows:

$$p_{xf} = -A_x(\pi/2 - \delta\phi_i) + p_x^C \sim \frac{E_0}{\omega}. \tag{A23}$$

From the latter we derive, using $\delta\phi_i \ll 1$ and Eq. (A12):

$$\delta\phi_i \sim \sqrt{\frac{2\omega p_x^C}{E_0}} \sim 2\sqrt{2}\sqrt{\frac{Z}{\sqrt{2I_p}}\left(\frac{E_0}{E_a}\right)^{1/3}\left(\frac{\omega}{I_p}\right)^{2/3}} \sim \frac{Z^{1/2}E_0^{1/6}\omega^{1/3}}{I_p^{5/6}}. \tag{A24}$$

[1] A. M. Perelomov, V. S. Popov, and V. M. Terent'ev, Zh. Eksp. Teor. Fiz. **51**, 309 (1966) [Sov. Phys. JETP **24**, 207 (1967)].

[2] A. M. Perelomov and V. S. Popov, Zh. Eksp. Teor. Fiz. **52**, 514 (1967) [Sov. Phys. JETP **25**, 336 (1967)].

[3] V. S. Popov, V. P. Kuznetsov, and A. M. Perelomov, Zh. Eksp. Teor. Fiz. **53**, 331 (1967) [Sov. Phys. JETP **26**, 222 (1968)] .

[4] V. S. Popov, Phys. Usp. **47**, 855 (2004).

[5] P. B. Corkum, Phys. Rev. Lett. **71**, 1994 (1993).

[6] W. Becker, F. Grasbon, R. Kopold, D. B. Milošević, G. G. Paulus, and H. Walther, Adv. Atom. Mol. Opt. Phys. **48**, 35 (2002).

[7] P. Agostini and L. F. DiMauro, Rep. Prog. Phys. **67**, 813 (2004).

[8] W. Becker, X. Liu, P. J. Ho, and J. H. Eberly, Rev. Mod. Phys. **84**, 1011 (2012).

[9] T. Brabec, M. Y. Ivanov, and P. B. Corkum, Phys. Rev. A **54**, R2551 (1996).

[10] G. L. Yudin and M. Y. Ivanov, Phys. Rev. A **63**, 033404 (2001).

[11] D. Comtois, D. Zeidler, H. Pépin, J. C. Kieffer, D. M. Villeneuve, and P. B. Corkum, J. Phys. B **38**, 1923 (2005).

[12] S. A. Kelvich, W. Becker, and S. P. Goreslavski, Phys. Rev. A **93**, 033411 (2016).

[13] C. I. Blaga, F. Catoire, P. Colosimo, G. G. Paulus, H. G. Muller, P. Agostini, and L. F. DiMauro, Nat. Phys. **5**, 335 (2009).

[14] F. Catoire, C. Blaga, E. Sistrunk, H. Muller, P. Agostini, and L. DiMauro, Laser Phys. **19**, 1574 (2009).

[15] W. Quan, Z. Lin, M. Wu, H. Kang, H. Liu, X. Liu, J. Chen, J. Liu, X. T. He, S. G. Chen, H. Xiong, L. Guo, H. Xu, Y. Fu, Y. Cheng, and Z. Z. Xu, Phys. Rev. Lett. **103**, 093001 (2009).

[16] C. Y. Wu, Y. D. Yang, Y. Q. Liu, Q. H. Gong, M. Y. Wu, X. Liu, X. L. Hao, W. D. Li, X. T. He, and J. Chen, Phys. Rev. Lett. **109**, 043001 (2012).

[17] B. Wolter, C. Lemell, M. Baudisch, M. G. Pullen, X.-M. Tong, M. Hemmer, A. Senftleben, C. D. Schröter, J. Ullrich, R. Moshammer, J. Biegert, and J. Burgdörfer, Phys. Rev. A **90**, 063424 (2014).

[18] J. Dura, N. Camus, A. Thai, A. Britz, M. Hemmer, M. Baudisch, A. Senftleben, C. D. Schröter, J. Ullrich, R. Moshammer, and J. Biegert, Sci. Rep. **3**, 2675 (2013).

[19] M. G. Pullen, J. Dura, B. Wolter, M. Baudisch, M. Hemmer, N. Camus, A. Senftleben, C. D. Schröter, R. Moshammer, J. Ullrich, and J. Biegert, J. Phys. B **47**, 204010 (2014).

[20] Q. Z. Xia, D. F. Ye, L. B. Fu, X. Y. Han, and J. Liu, Sci. Rep. **5**, 11473 (2015).

[21] B. Wolter, M. G. Pullen, M. Baudisch, M. Sclafani, M. Hemmer, A. Senftleben, C. D. Schröter, J. Ullrich, R. Moshammer, and J. Biegert, Phys. Rev. X **5**, 021034 (2015).

[22] K. Zhang, Y. H. Lai, E. Diesen, B. E. Schmidt, C. I. Blaga, J. Xu, T. T. Gorman, F. Légaré, U. Saalmann, P. Agostini, J. M. Rost, and L. F. DiMauro, Phys. Rev. A **93**, 021403 (2016).

[23] E. Diesen, U. Saalmann, M. Richter, M. Kunitski, R. Dörner, and J. M. Rost, Phys. Rev. Lett. **116**, 143006 (2016).

[24] J. B. Williams, U. Saalmann, F. Trinter, M. S. Schöffler, M. Weller, P. Burzynski, C. Goihl, K. Henrichs, C. Janke, B. Griffin, G. Kastirke, J. Neff, M. Pitzer, M. Waitz, Y. Yang, G. Schiwietz, S. Zeller, T. Jahnke, and R. Dörner, J. Phys. B **50**, 034002 (2017).

[25] C. Liu and K. Z. Hatsagortsyan, Phys. Rev. Lett. **105**, 113003 (2010).

[26] T.-M. Yan, S. V. Popruzhenko, M. J. J. Vrakking, and D. Bauer, Phys. Rev. Lett. **105**, 253002 (2010).

[27] A. Kästner, U. Saalmann, and J. M. Rost, Phys. Rev. Lett. **108**, 033201 (2012).

[28] C. Lemell, K. I. Dimitriou, X.-M. Tong, S. Nagele, D. V. Kartashov, J. Burgdörfer, and S. Gräfe, Phys. Rev. A **85**, 011403 (2012).

[29] W. Becker and D. B. Milošević, J. Phys. B **48**, 151001 (2015).

[30] T. Keil, S. V. Popruzhenko, and D. Bauer, Phys. Rev. Lett. **117**, 243003 (2016).

[31] L. V. Keldysh, Zh. Eksp. Teor. Fiz. **47**, 1945 (1964) [Sov. Phys. JETP **20**, 1307 (1965)].

[32] F. H. M. Faisal, J. Phys. B **6**, L89 (1973).

[33] H. R. Reiss, Phys. Rev. A **22**, 1786 (1980).

[34] J. Z. Kamiński, A. Jaroń, and F. Ehlotzky, Phys. Rev. A **53**, 1756 (1996).

[35] M. Kübel, M. Arbeiter, C. Burger, N. G. Kling, T. Pischke, R. Moshammer, T. Fennel, M. F. Kling, and B. Bergues, J. Phys. B **51**, 134007 (2018).

[36] S. V. Popruzhenko, G. G. Paulus, and D. Bauer, Phys. Rev. A **77**, 053409 (2008).

[37] S. V. Popruzhenko and D. Bauer, J. Mod. Opt. **55**, 2573 (2008).

[38] L. Torlina and O. Smirnova, Phys. Rev. A **86**, 043408 (2012).

[39] L. Torlina, M. Ivanov, Z. B. Walters, and O. Smirnova, Phys. Rev. A **86**, 043409 (2012).

[40] J. Kaushal and O. Smirnova, Phys. Rev. A **88**, 013421 (2013).

[41] J. Z. Kamiński, Acta Phys. Pol. A **66**, 517 (1984).

[42] H. K. Avetissian, A. G. Markossian, G. F. Mkrtchian, and S. V. Movsissian, Phys. Rev. A **56**, 4905 (1997).

[43] H. K. Avetissian, K. Z. Hatsagortsian, A. G. Markossian, and S. V. Movsissian, Phys. Rev. A **59**, 549 (1999).

[44] F. Cajiao Velez, K. Krajewska, and J. Z. Kaminski, Phys. Rev. A **91**, 053417 (2015).

[45] F. C. Velez, K. Krajewska, and J. Z. Kaminski, J. Phys.: Conf. Ser. **691**, 012003 (2016).

[46] M. Li, J.-W. Geng, M. Han, M.-M. Liu, L.-Y. Peng, Q. Gong, and Y. Liu, Phys. Rev. A **93**, 013402 (2016).

[47] S. Augst, D. Strickland, D. D. Meyerhofer, S. L. Chin, and J. H. Eberly, Phys. Rev. Lett. **63**, 2212 (1989).

[48] J. Z. Kaminski, F. C. Velez, and K. Krajewska, arXiv:1807.08285.